Noname manuscript No.
(will be inserted by the editor)

Motor-Induced Structuring of Tactile Sensory Information for Category Formation in Robotics Palpation.

Luca Scimeca [1] · **Perla Maiolino** [1] · **Ed Bray** [1] · **Fumiya Iida** [1] ·

Received: date / Accepted: date

Abstract This paper investigates the effects that motor-induced contact-based interactions with a soft phantom have on tactile sensor information. We embed a capacitive tactile sensor on a robotic arm to probe a soft phantom and detect possible hard inclusions. A combination of PCA and K-Means clustering is used to: first, reduce the dimensionality of the spatiotemporal data obtained through the probing of each area in the phantom; second categorize the re-encoded data into a given number of categories. Results show that appropriate probing interactions can be useful in compensating for the quality of the data, or lack thereof. Moreover, it is possible to use various probing strategies to vary the similarity relationships between different objects, and induce orderings in the perceived categories.

Keywords Robotic palpation, Tactile sensing, Motor-Induced sensing, Sensory-Motor coordination

1 Introduction

In the last decades, substantial efforts have been made in enhancing the sensing capabilities of robots by providing them with a sense of touch [3,4]. Haptic sensing differs from other modalities, such as vision, in virtue of its tight coupling with, and need of, physical interactions. Haptic sensing requires direct physical contacts with sensing targets, inducing spatio-temporal force patterns on the contact surface, which may or may not be the consequence of motor behaviors of the robots. Furthermore, force patterns are significantly related to the shape and mechanical properties of sensing surfaces (e.g. stiffness) and the target objects [7,21].

In medical palpation diagnosis, for example, given the nature of soft tissues in the human body, haptic perception plays a fundamental role [18]. Here, practitioners necessitate the use of different palpation strategies according to the task, whether this is an organ to examine, finding cancerous inclusions or investigating their characteristics. In this context, contacts and physical interactions are the basis of rich sensory stimuli, with which practitioners can judge the conditions of target areas [1,5,26]. Indeed, previous research has focused on the use of haptics for RMIS and medical training [13]. These systems, currently based on vision, can be augmented by haptic, improving the surgeons' ability to detect the mechanical properties of touched organs, and help in the detection of tumors and lumps [8].

The strong dependence between the somatosensory system and motor actions in human palpation has been investigated in relation to the development of robotic palpation systems for detection of tumors and lump inclusions [9,10,22,27] and it is considered of primary importance in categorization [16]. In this context, we refer to categorization as the process corresponding to the separation and association of sensor information into groups. The number of groups, to divide the sensor space into, sets the level of abstraction intended for the understanding of the sensor information.

This work was funded by the UK Agriculture and Horticulture Development Board and by The United Kingdom Engineering and Physical Sciences Research Council (EPSRC) MOTION grant [EP/N03211X/2].

Luca Scimeca
E-mail: ls769@cam.ac.uk

Perla Maiolino
E-mail: pm640@cam.ac.uk

[1] Bioinspired Robotic Lab, Engineering Department, University of Cambridge, Cambridge UK

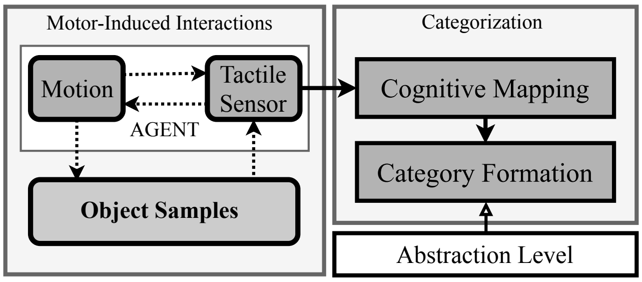

Fig. 1: Theoretical Framework.

The importance of categorization has previously been emphasized [6], and the use of active interactions to solve the categorization problem has been explored in previous research [14,16,25]. Considering the problem of categorization in the scenario of robotic palpation systems, much is still unclear. This paper addresses two related problems. First, we wish to understand how motor actions can aid in the separation and categorization of tactile sensor information. Research has previously shown that motor actions can introduce structure in sensory information [12,17,23], but it is yet to be understood which principles guide the emergence of such structure. Second, as later shown in this paper, knowing the task to solve may not be enough to understand which physical interaction strategy is appropriate to use, or predict its effects to the tactile information. Here, instead, it is first necessary to understand the properties of the objects in interaction with the agent and the level of abstraction intended for the categorization.

In order to address the above problems this paper investigates the processing of sensor signals based on dimensionality reduction and clustering. We explore the way active physical interactions with a soft body affect the structure of haptic spatio-temporal information. Moreover, we observe how the properties of the probed areas, and the number of categories imposed in the categorization, influence the structuring induced by the physical interaction.

The paper is organized as follows: In Section 2 we describe the theoretical framework for this work. In Section 3 we describe the methods used, starting from the experimental set-up in section 3.1, to the acquisition of tactile data and performed motor-induced interactions in sections 3.2 and 3.3. In section 4 we report the results of the experiments followed by the conclusion in section 5.

2 Theoretical Framework

In this paper we consider the framework in Fig. 1. In the framework, an agent retrieves tactile sensor information while interacting with samples of objects, defined by a task. In this context, the tactile information is directly influenced by the motor-induced interactions with the samples. A categorization system allows for the information to be: first, re-encoded into a meaningful, lower-dimensional space (Cognitive Mapping); second, differentiated into useful categories (Category Formation). The abstraction level corresponds to the number of categories that should be observed in the sensor information and has a direct influence on the significance of the formed categories. At its limit, 2 categories might be too coarse to be useful in capturing differences amongst different types of objects, while a number of categories equal to the number of object samples is impractical in identifying any similarities amongst them, and therefore amongst similar objects. The direct influence of the motor-induced interactions to the tactile information, if substantial, should be observable in the category formation process.

2.1 Task and Motor-Induced Interaction

In the framework considered, the agent is an embodied system equipped with a tactile sensor, and capable of performing probing actions. The motor-induced interactions consist of physical contact-based probing strategies with target areas in a soft phantom. The areas in the soft phantom differ in that each may or may not contain hard inclusions.

As exemplified in Fig. 2, an experiment consists of an agent probing a preselected phantom with a chosen probing strategy. The agent iteratively selects a target area in the phantom to probe, and performs the chosen probing strategy for the experiment (described by Θ) while acquiring and storing tactile information. After probing all intended areas the stored sensor information can undergo categorization.

2.2 Categorization

2.2.1 Cognitive Mapping

A process is needed to reduce the high dimensionality of the spatiotemporal data acquired through the tactile sensor, while interacting with the environment. We define a tactile image sequence as a series of tactile sensor readings taken at set intervals, and concatenated into a single array. After acquiring tactile image sequences

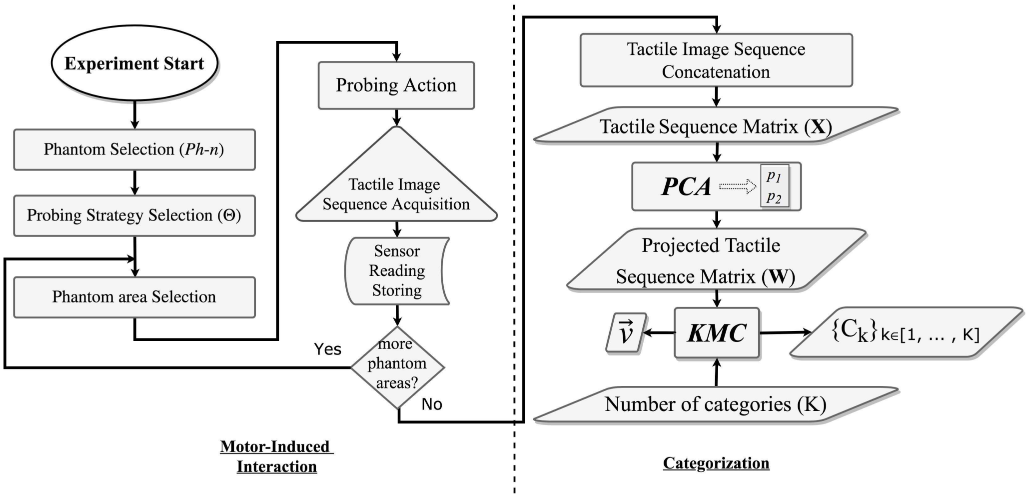

Fig. 2: Implementation steps of the Theoretical Framework.

for each probed location, we use Principal Component Analysis projection (PCA) [24] to reduce the dimensionality of the acquired data [11].

For a set of N different locations in a phantom, let $\mathbf{X}$ be a $(N \times D)$ matrix where each unique tactile image sequence for a probed location is a D dimensional row $(D \gg 2)$ in the matrix. The dimension of D, then, will be strictly dependent on the probing strategy and on the interval at which the agent captures each tactile image within the sequence.

After obtaining the tactile image sequences matrix $\mathbf{X}$, we begin the process by finding the average tactile sequence $\boldsymbol{\mu}$ as:

$$\boldsymbol{\mu} = \frac{1}{N}\sum_{i=1}^{n}\mathbf{x}_i \tag{1}$$

where $\mathbf{x}_i$ is a column vector corresponding to the i^{th} row in $\mathbf{X}$. We compute a $(D \times D)$ scatter matrix $\mathbf{S}$ as:

$$\mathbf{S} = \sum_{i=1}^{N}(\mathbf{x}_i - \boldsymbol{\mu})(\mathbf{x}_i - \boldsymbol{\mu})^T \tag{2}$$

and use Single Value Decomposition to factorize $\mathbf{S}$ into

$$\mathbf{S} = \mathbf{Q}\boldsymbol{\Lambda}\mathbf{Q}^{-1} \tag{3}$$

where $\mathbf{Q}$ is a matrix such that each column q_j corresponds to an eigenvector of $\mathbf{S}$, and each element λ_{jj} in the diagonal matrix Λ is its corresponding eigenvalue. We list the eigenvectors in ascending order of eigenvalue and select the first two in the list. Let $\mathbf{p}_1$ and $\mathbf{p}_2$ be the selected eigenvectors obtained from PCA.

We form a $(D \times 2)$ projection matrix $\mathbf{P}$ as:

$$\mathbf{P} = \left[\mathbf{p_1}^T, \mathbf{p_2}^T\right] \tag{4}$$

where $\mathbf{p_1}^T$ and $\mathbf{p_2}^T$ are column vectors in $\mathbf{P}$.

Finally, we project the D-dimensional row vectors in $\mathbf{X}$ onto a 2-dimensional subspace by:

$$\mathbf{W} = \mathbf{X} \cdot \mathbf{P} \tag{5}$$

where $\mathbf{W}$ is a $(N \times 2)$ matrix. Each row in the matrix is a 2-dimensional *encoding* of a tactile image sequence for a probed location.

2.2.2 Category Formation and Abstraction Level

To observe the effects of the probing strategies to the tactile sensor information we wish to have a process to categorize the re-encoded sensor information. We use K-Means Clustering (KMC) to find clusters in the data, where each found cluster will represent a potential category of inclusion types. The abstraction level is set by the number of clusters we wish to find in the data. We initialize the KMC algorithm with random centroids, and split the re-encoded sequences in $\mathbf{W}$ into K clusters by:

$$\mathbf{v} = KMC_K(\mathbf{W}) \tag{6}$$

The resulting $\mathbf{v}$ is an N-dimensional array, where each element $\mathbf{v}_i \in \{1, ..., K\}$, and $\forall i \in \{1, \ \dots \ , N\} \ \exists j \in \{1, \ \dots \ , N\} : \ i \neq j \ \wedge \ v_i \neq v_j$ (Fig. 2); in other words, none of the resulting clusters can contain all the sample areas in the phantom.

In general $\mathbf{v}_i = k$ only if the i^{th} tactile image sequence belongs to cluster k, thus the $\mathbf{v}$ vector contains the cluster membership of each probed location in the initial set.

To avoid cluster anomalies due to the random centroid initializations we run the KMC algorithm three

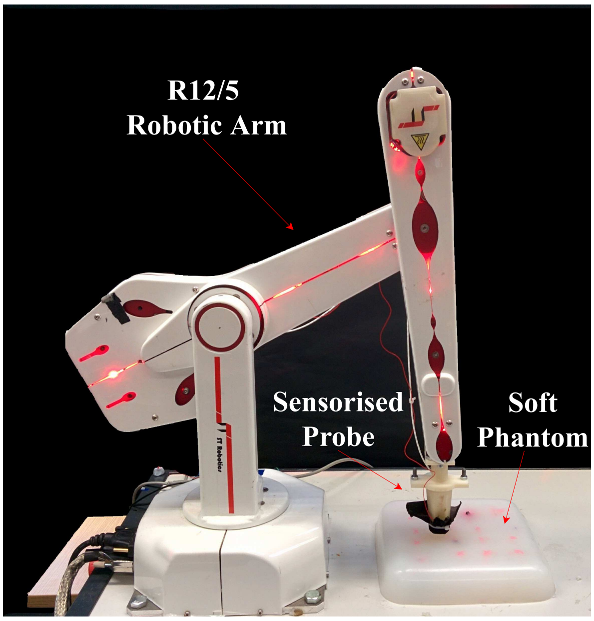

(a) Robot set-up

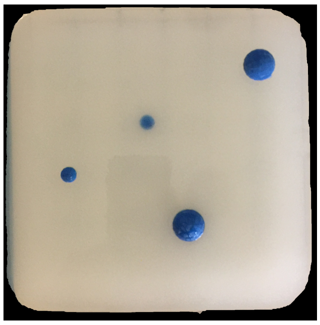

(b) *Ph*-1

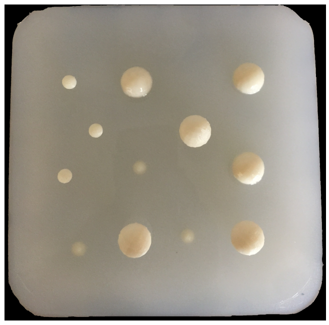

(c) *Ph*-2

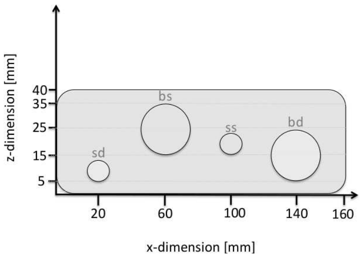

(d) Inclusion types

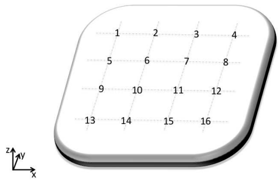

(e) Phantom grids

Fig. 3

times and discard the clustering attempt if, after convergence, any of the three cluster guess vectors differs from any other. At the end of the clustering process a list of centroids C is obtained, uniquely dividing the space into K categories (2). In this context, the cluster assignments for each probed location is largely dependent on the probing strategy employed.

3 Methods

To realize the described framework, we arrange an experimental scenario where a robotic arm interacts with a soft phantom through a probe equipped with a tactile sensor.

3.1 Soft Phantom and Robot Set-Up

We built two 160x160x40mm soft phantom organs using Ecoflex 00-10[2] from Smooth-on. The phantom organs are divided in 16 locations disposed in a coarse grained grid system as shown in Fig. 3e. Each location in the phantoms may or may not contain hard inclusions. An inclusion consists of a 3D-printed hard, spherical bead, embedded in the phantoms at a depth of either 5mm or 15mm, and having a diameter of 7mm or 20mm (Fig. 3d). Hereafter we may refer to a 7mm inclusion placed at a depth of 5mm as *SS* (Small-Shallow), a 20mm inclusion placed at 5mm as *BS* (Big-Shallow), a 7mm inclusion placed at 15mm as *SD* (Small-Deep), a 20mm inclusion placed at 15mm as *BD* (Big-Deep) and an area containing no hard inclusions as *NA*.

The experiments were performed on two phantoms: *Ph*-1, containing 12x*NA*, 1x*SD*, 1x*SS*, 1x*BS*, 1x*BD* (Fig. 3b); and *Ph*-2, containing 4x*NA*, 3x*SD*, 3x*SS*, 3x*BS*, 3x*BD* (Fig. 3c).

We 3D-printed a custom-made end-effector and integrated a capacitive tactile sensor onto its surface to retrieve *tactile images* during the probing experiments (Fig. 4b). The printed end-effector, coupled with the tactile sensor, was mounted onto an ST-Robotics R12/5 robotic arm[3] (Fig. 3a).

3.2 Tactile Sensor Technology and Data Acquisition

High spatial resolution is a crucial component of the sensor technology necessary for the analysis in this paper. The tactile sensor used is described in [20]. The adopted sensing mode is based on the capacitive transduction principle. A capacitive transducer (i.e., a tactile element, or *taxel*) is organized in a layered structure: the lower layer consists of the positive electrode, which is mounted on a Flexible Printed Circuit Board (FPCB); a small air chamber act as dielectric and the

[2] https://www.smooth-on.com/products/ecoflex-00-10/

[3] http://www.robotshop.com/uk/st-robotics-r12-5-axis-articulated-robot-arm.html

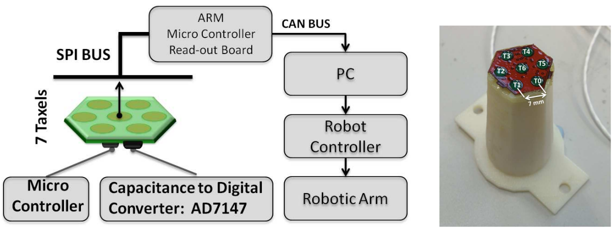

(a) (b)

Fig. 4: (a) The CySkin technology architecture. The hexagonal patch is connected to a Intelligent Hub Board (IHB) that collect the tactile sensor data and send them to the PC through a CAN bus. (b) The sensorised probe coupled with the CySkin patch used for the experiments.

upper layer is a ground plane made with conductive lycra. The tactile sensor is made up of a number of taxels geometrically organized in triangular modules.

In the current prototype, each module hosts 7 taxels (Fig. 4b), as well as the Capacitance to Digital Converter (CDC) chip (namely, the AD7147 from Analog Devices) for converting capacitance values to digital. The CDC chip can measure variations in capacitance values with 16 bits of resolution. All the modules are interconnected and communicate through an SPI bus to a read-out board which performs a preliminary processing of the tactile sensor data and send them to the PC through CAN bus (Fig. 4a) with a sensitivity of $0.32fF$.

In this context, the normal forces exerted on the sensor produce variations in capacitance values reflecting the varied pressure over the taxel positions. A sensor reading, or tactile image, from the tactile sensor described is produced at $20Hz$, and corresponds to a 7-dimensional array, where each element contains the capacitance variation value of the corresponding taxel.

3.3 Probing Strategies

We control the r12/5 robotic arm open-loop in Cartesian coordinates. A teach-pendant was used to manually teach the robot the x-y location of the areas to probe. We use the stored end-effector positions in the subsequent control algorithm, where the robot automatically probes each location using the preferred probing strategy. We differentiate between two qualitatively different types of probing strategies, summarized in Fig. 5: vertical and rotatory.

First, the vertical probing strategy is performed with the probe aligned vertically and plunged directly down into the phantom at 0.5 mm increments. After each increment, the robot briefly pauses to allow a tactile image to be recorded before continuing with the next movement. This continues until the probe is at a depth d below the surface of the silicon, whereupon it stops recording and returns to a neutral position 10 mm above the surface in a single movement.

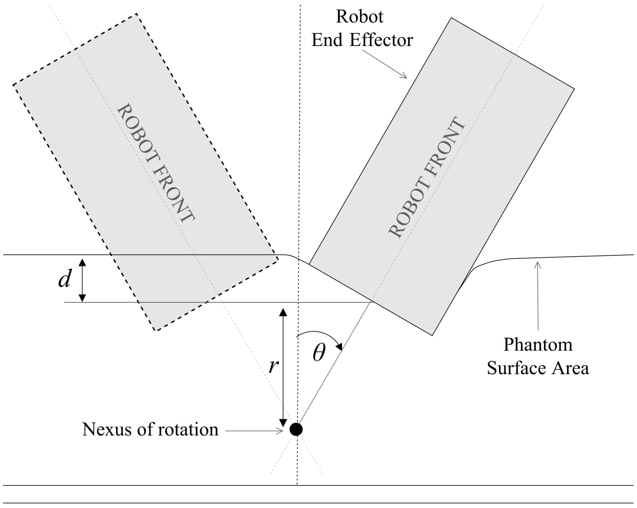

Fig. 5: Diagram of the two probing motions employed. The d and r parameters fully specify the type of motion employed.

Second, the rotary motion is performed with the robot d mm below the surface of the silicone, rotating about a nexus point r mm away in the vertical direction. To reach the initial position of this motion strategy, the robot moves vertically downward from its rest position, until it reaches the position set by d. Hence, a nexus point r distant from the end effector is assumed, and the robot rotates about it in the $+\theta$ direction until it is at an angle of 30° from its initial, vertical, position. Here, the palpation action can begin. The probe rotates in the $-\theta$ direction at 1° increments, recording a tactile image after each step. Once the probe has rotated of 60° it stops recording, and returns to its rest position 10 mm above the surface of the silicone.

In general, a probing strategy can be uniquely identified by a depth d and a radius r, thus:

$$\Theta = \begin{Bmatrix} d \\ r \end{Bmatrix}, \tag{7}$$

where if $r = 0$, the probing motion will be vertical, while if $r > 0$ the probing takes place via the rotatory strategy (Fig. 5).

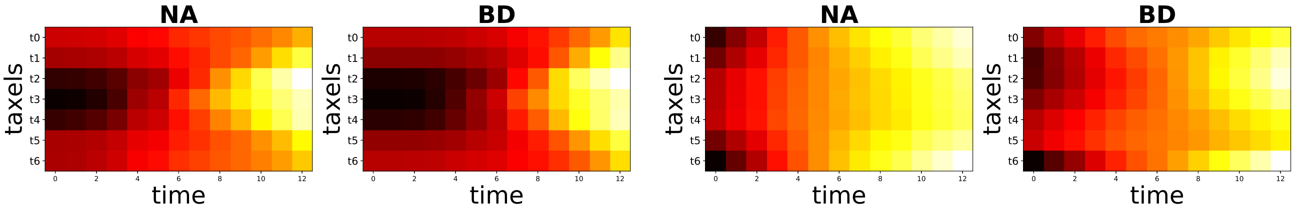

(a) $\Theta = \left\{ {6.5 \atop 0} \right\}$ (b) $\Theta = \left\{ {19.5 \atop 0} \right\}$

Fig. 6: The raw spatiotemporal tactile image sequences, as captured when probing Ph-2 vertically at varying depths, in an area containing no hand inclusion, and an area containing a 15mm inclusion placed 20mm deep. Each tactile image sequence corresponds to a re-shaped x_i.

3.4 Experimental Procedure

We execute 180 experiments, each of which sees the robot probing all 16 areas of Ph-1 or Ph-2 with the preferred Θ parameters. The experiments are carried out for all combinations of $d \in [6.5mm, ..., 20.5mm]$ at $1mm$ increments and $r \in [0mm, 10mm, 12mm, 14mm, 16mm]$. The bounds were chosen to reach the minimal/maximal experimentally feasible probing depth and rotation with the robotic arm, and the devised soft phantoms.

For each of the experiments, after the probing has ended, the time-concatenated data is used to form the tactile image sequence matrix described (see Section 2.2.1). The matrix can then be used to re-encode the tactile sensor information for each probed location into a lower dimensional space ($Cognitive\ Mapping$). After clustering, each probed location will be differentiated into one of a predetermined number of categories ($Category\ Formation$).

4 Results

The following sections will progressively analyze the described framework, starting from the dimensionality reduction process (PCA), to the repercussions of motor-induced interactions to categorization (KMC).

4.1 Sound Dimensionality Reduction

One of the principal components of the proposed framework is the reduction of the high dimensional spatiotemporal tactile information, into re-encoded lower dimensional data. An example of the acquired tactile information is shown in Fig. 6. Without knowing which category each tactile sequence vector $\mathbf{x_i}$ belongs to, it is impossible to assess the quality of dimensionality reduction from $\mathbf{X}$ to $\mathbf{W}$. However, it is feasible to maximize the information retention in the original tactile sensor data.

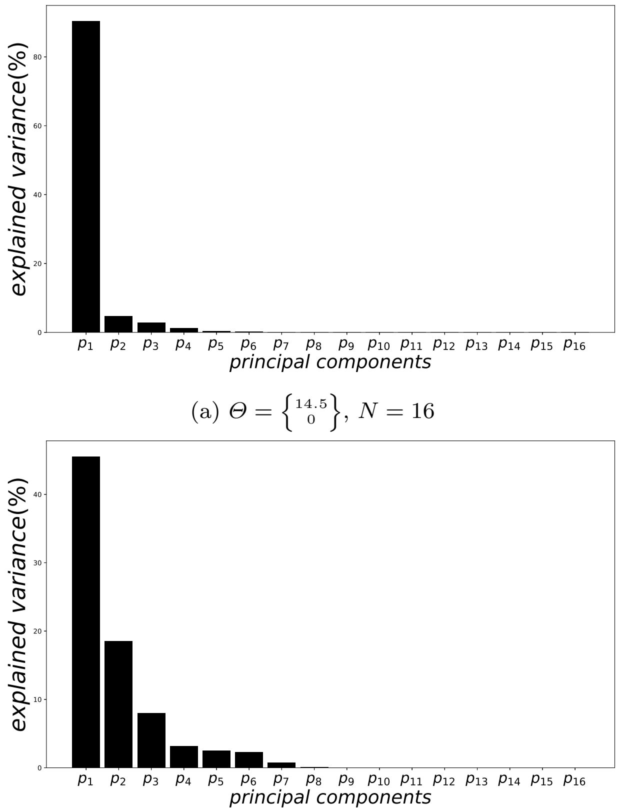

(a) $\Theta = \left\{ {14.5 \atop 0} \right\}$, $N = 16$

(b) $\Theta = \left\{ {18.5 \atop 12} \right\}$, $N = 8$

Fig. 7: The explained variance of each principal component when projecting the $\mathbf{X}$ matrix belonging to two different experiments where both the number of probed areas in Ph-2, to base the PCA projection on, and the Θ parameters where changed.

The explained variance can be thought of as a measure of the information captured by the PCA subspace after projection. As the eigenvalues in Λ (see Eq. 3) are proportional to the variance captured by the corresponding PCA principal components, we can compute the explained variance τ_i for the principal component

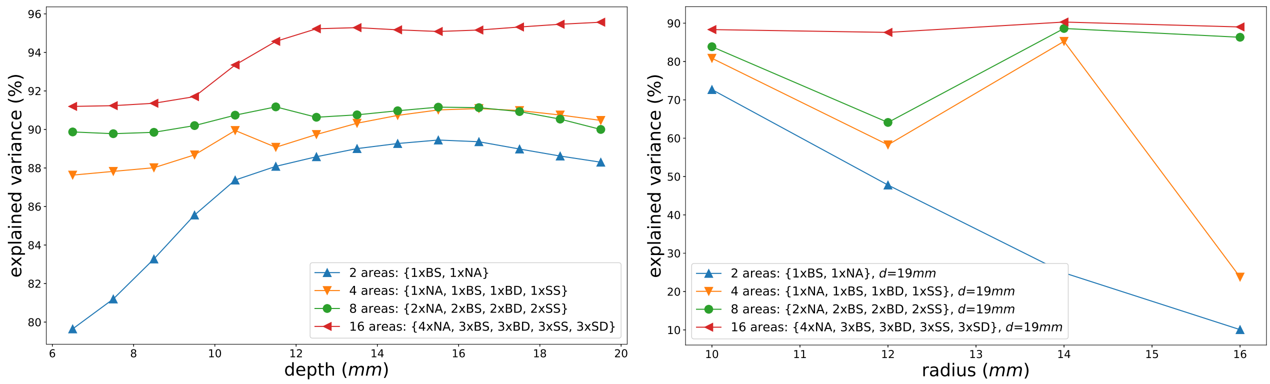

(a) *Ph*-2: Vertical Probing (b) *Ph*-2: Rotational Probing

Fig. 8: The change in explained variance by the 2D PCA subspace projection, when probing vertically (a) and through the rotatory motion (b), changing the number of samples used to find the principal components (N in $\mathbf{X}$, see Section 2.2.2).

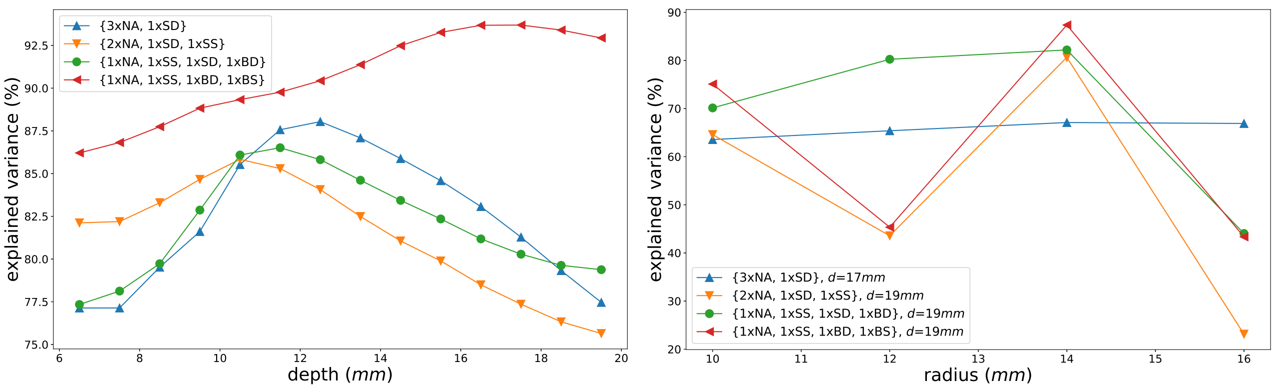

(a) *Ph*-2: Vertical Probing (b) *Ph*-2: Rotational Probing

Fig. 9: The change in explained variance by the 2D PCA subspace projection, when probing vertically (a) and through the rotatory motion (b), changing the quality of the samples used to find the principal components, while maintaining their number constant.

$\mathbf{p_i}$ as:

$$\tau_i = \frac{\lambda_i}{\sum_{j=1}^{N} \lambda_j} \tag{8}$$

where λ_i is the eigenvalue corresponding to the i^{th} principal component. Here, τ_i is a measure of the proportion of variance in the data, captured along the direction the principal component $\mathbf{p_i}$ in the original sensor space.

Figure 7 shows the explained variance of each $\mathbf{p}_i$, after the robot probed *Ph*-2 in two different experiments where both Θ and the number of probed areas used for the projection (N) were varied. As clear from the figure, the number of probed areas and the Θ choice significantly affect the distribution of the sensor data in its original D space. In one case, the sensor data is mainly spread along 7 axis ($\mathbf{p}_1 - \mathbf{p}_7$) (Fig. 7b), making it unsuitable for dimensionality reduction. In the other, instead, $\mathbf{p}_1$ captures the majority of the information in the data (Fig. 7a). The figure suggests the suitability of the tactile information to the drastic reduction in dimensionality is dependent both on the properties of the probed areas, and probing strategy employed.

We further explore the way the probing strategy, and the properties of the probed areas in the phantom, affect the amount of information retained after dimensionality reduction. The explained variance achieved prior to categorization is $I = \tau_1 + \tau_2$. Fig. 8b shows the explained variance trends when the number of probed areas used for *PCA* projection varies. When the number of probed areas in maximal (16 areas, red plot in Fig. 8b), the influence of Θ is negligible. Conversely, with less data to base the *PCA* projection on (2 areas, blue plot in Fig. 8b), the choice of Θ can be the sole determinant to induce structure in the data. A second interesting phenomenon can be observed in Fig. 8a, when comparing the explained variance obtained after projecting $\mathbf{X}$ based on 4 vs 8 probing areas in the phantom (yellow vs green plots). Here, the agent retains more information, even when basing the projection on less data, if the employed probing is vertical and at a depth of at least $17.5mm$. The plot suggests that proper physical interaction can help information retention in the absence of enough data.

Ultimately, we observe the influence of the quality of the data samples to the information retention after PCA projection. Fig. 9a shows how in presence of very diverse inclusion types (left triangle plot), the effects of the vertical probing strategy Θ to I is negligible. The presence of very diverse data, in fact, is useful for PCA to find good projection axis. In absence of good data, or non-diverse inclusion types, instead, appropriate interaction can minimize information loss (peaks in Fig. 9a and 9b). In the figures, it is possible to see how the least diverse set of samples can yet induce the tactile information to retain most of the information when the phantom is appropriately probed (peak in triangle plot, Fig. 9a).

4.2 Information Structure and Silhouette Coefficient

For the unsupervised clustering algorithm to be able to find meaningful clusters in the re-encoded tactile data, it is necessary that the data exhibits structure. We use a metric of structure tightly connected to the type of clustering utilized in this paper, i.e. the silhouette score [19]. The silhouette score $s(i)$ for cluster i can be computed as:

$$s(i) = \frac{b(i) - a(i)}{\max(a(i),\ b(i))} \tag{9}$$

where $a(i)$ is the mean intra-cluster distance of cluster i, and $b(i)$ is its mean nearest-cluster distance (Fig. 10). We will refer to the silhouette score s as the average score for each cluster found by KMC, i.e.:

$$s = \frac{\sum_{i=1}^{K} s(i)}{K} \tag{10}$$

The score will thus be a number $s \in [-1, 1]$, where data exhibiting more structure will score higher s values.

Similarly to the previous sections we wish to observe the effects of changing the Θ parameters to the structure of the information after PCA projection. Fig. 11 and Fig. 12 both show how the change in Θ influences the silhouette score. This influence, however, is primarily dependent on N and the diversity of the inclusions probed, as suggested by the change in trends

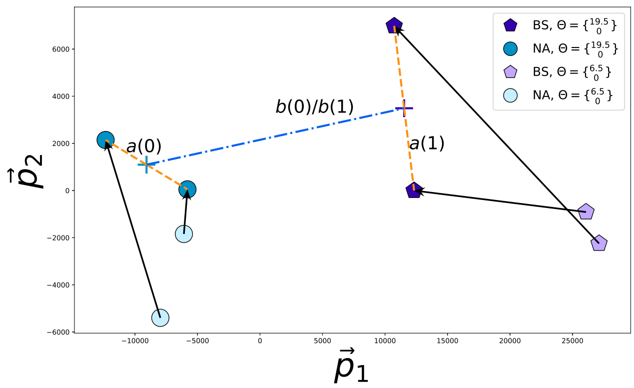

Fig. 10: The change in position for the 2D PCA projected NA and BS samples when probing the phantom vertically at a depth of $6.5mm$ and $19.5mm$. The yellow and blue line show the two parameters on which the silhouette score is based, i.e. intra-cluster distance and nearest cluster distance respectively.

of the plots in each of the figures. Fig. 11a shows that little structure emerges when probing Ph-2 vertically too superficially or too deeply. In both cases, in fact, the sensor response is uniformly too moderate or too steep to have any variation from an area of the phantom to another, thus inducing no variation in the information. Fig. 11b, instead, shows how, when in absence of enough data samples (2 areas, blue plot), a correct choice of Θ can be the sole determinant for good or bad structure in the information. In Fig. 12a and Fig. 12b, interestingly, it is shown how even without much diversity in the inclusion types, good structure can emerge when the phantom is probed appropriately ($\Theta = \left\{ {16.5 \atop 0} \right\}$ or $\Theta = \left\{ {14.5 \atop 16} \right\}$).

At last, we investigate the influence of the number of clusters K to the structure of the information s. The number of clusters sets the level of abstraction that the robot may wish to have to make use of the tactile information, and directly affect the interpretation of the emerging clusters. We choose three varying number of clusters: $K = 2$, presence vs. absence of an hard inclusion; $K = 3$, absence vs. small vs. large inclusion; $K = 5$, all inclusion types. Fig. 13 shows the trends when probing the soft phantom vertically at varying depths and changing K in the KMC algorithm. The emerging clusters present different structural properties. The different trends in the figure suggest how K directly affect the way the probing strategy influences the structure of the data. Interestingly, probing at a deeper depth increasingly helps to sense inclusions, or detect their size. To dissociate between all different inclusion types, instead, an optimal probing depth is found for $d = 14.5mm$, after which the increasingly high sensor

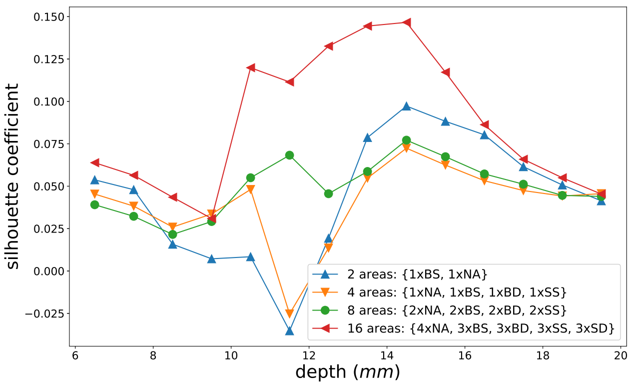

(a) *Ph*-2: Vertical Probing

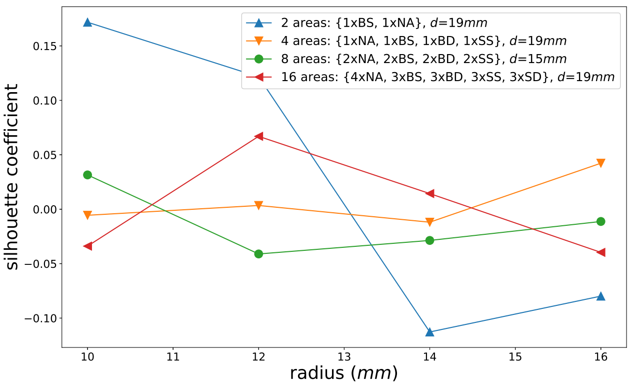

(b) *Ph*-2: Rotational Probing

Fig. 11: The change in silhouette coefficient by the 2D PCA subspace projection, when probing vertically (a) and through the rotatory motion (b), changing the number of samples used to find the principal components (N in $\mathbf{X}$, see Section 2.2.1).

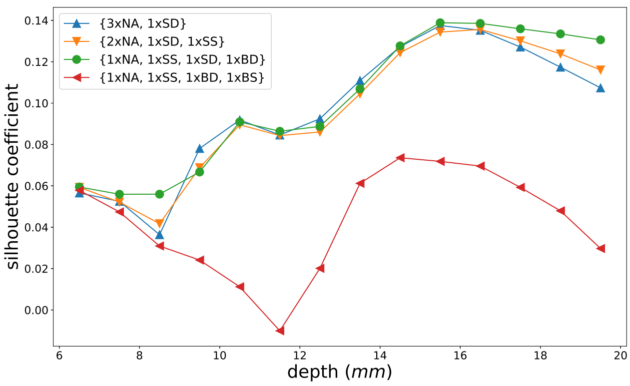

(a) *Ph*-2: Vertical Probing

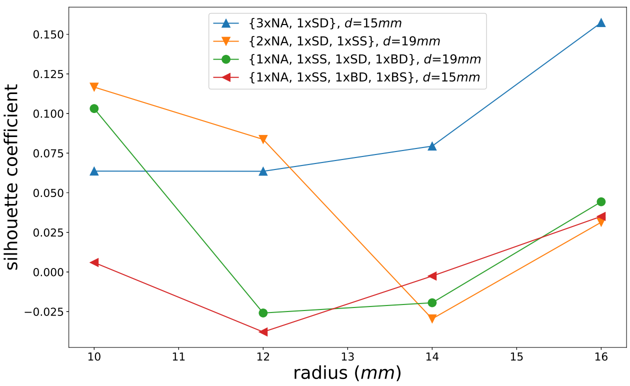

(b) *Ph*-2: Rotational Probing

Fig. 12: The change in silhouette coefficient by the 2D PCA subspace projection, when probing vertically (a) and through the rotatory motion (b), changing the quality of the samples used to find the principal components, while maintaining their number constant.

response converges, and renders the clusters less separable, thus decreasing the values of s.

4.3 Motion influence on Cognitive Maps

Predicting the effects of Θ to the low-level encoding of the information in $\mathbf{W}$ is a highly complex process. Understanding such effects, however, would allow an agent to appropriately choose a Θ when solving the probing task.

To understand this relationship we make a plot of the cognitive maps for each set of motion parameters in Θ and observe how the encoding of each probed area changes according to the probing strategy used. Here, to have a better understanding of the motion effects, we perform the experiment on the least cluttered phantom, i.e. *Ph*-1 (Fig. 3c), which would suffer less from disturbances due to the vicinity of adjacent inclusions. Figure 14a and 14b show the plots corresponding to probing the phantom vertically at the minimal and maximal experimental depth. By increasing the depth of probing, two very interesting effects take place: one, nearest cluster distance $b(i)$ between almost all types of inclusions increases, allowing for better dissociation of diverse tactile information; two, the intra cluster distance $a(i)$ between any two probing areas with the same type of hard inclusion decreases, allowing for each possible phantom inclusion type to be better represented.

Extending the analysis to the rotational probing strategy we can similarly observe the effects of changing the parameters in Θ from their minimal to their maximal experimental values. Interestingly, when employing the rotational strategy, the generated tactile informa-

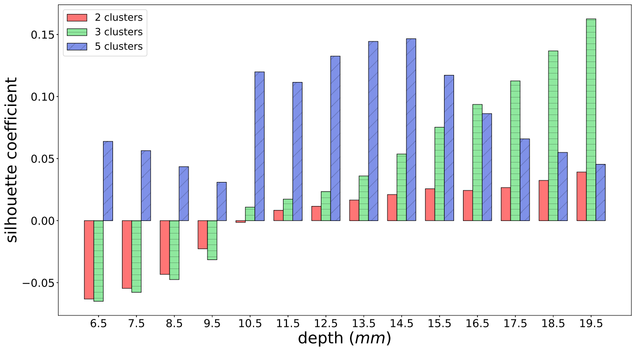

Fig. 13: The silhouette score of PCA projected tactile sensor information for every probing area in the soft phantom, when performing the probing action at different depths, and over varying number of clusters.

tion presents a structured layout, by which it is already possible to dissociate one stimulus type from another. In this scenario, then, the effect of the rotational parameter r to the structure of the data s appears to only mildly act upon the nearest-cluster distance parameter (Fig. 15a to Fig. 15b). The effect of increasing d, instead, confirms the hypothesis by which the probing depth influence acts upon the intra cluster distance of each stimulus type.

The effect of the depth parameter can be attributed to the strength in response of the sensorised probe. The tactile sensor, in fact, detects pressure levels on its surface. When probing the phantom at the minimum depth, the pressure registered by the sensor is mostly due to the elastic response of the Ecoflex 00-10 soft phantom, almost independently from the presence or absence of inclusions in the probed area. As the depth increases, the elastic response is influenced by the non-elasticity of the hard inclusion, should there be one in the probed area. We hypothesize this influence can be captured by the sensor response in three ways: first, the response should be higher when inclusions are present in the probed area; second, the sensor's increase in detected pressure should arise at slightly different sample intervals depending on where the inclusion is placed in the phantom (deep vs shallow inclusion); third, the area of the response should vary depending on the size and depth of the inclusion.

In this framework, an acceptable probing depth is one which neither saturates the sensor response in each area, nor fails to detect changes in pressure when the probed area contains non-elastic inclusion. The task of dissociating amongst all different types of inclusions is optimized (i.e. maximal silhouette score) for $\Theta = \left\{ {12.5 \atop 0} \right\}$ in *Ph*-1 and $\Theta = \left\{ {14.5 \atop 0} \right\}$ in *Ph*-2.

4.4 Categorization and Similarity Abstractions

In robotics palpation, proper motor-induced interaction can help in the dissociation of tactile information, such that the emerging clusters can be meaningful with respect to solving a task (e.g. finding hard inclusions in a soft phantom). Besides dissociating amongst different object types, however, another fundamental, yet usually neglected, fragment of information is related to the similarity associations between clusters. The distances between found clusters in the 2D re-encoded tactile information subspace, in fact, grants the agent the possibility to associate types of objects, and order or rank them based on such association.

In the context of probing a soft phantom to find hard inclusions, for example, the agent might need to prioritize possible findings based on the depth of the inclusion, e.g. [*NA*, *SD/BD*, *SS/BS*], we'll refer to this as rank-1. In a different scenario where the size of the hard inclusion should take priority over its depth, the ranking might, for example, change to [*NA*, *SD/SS*, *BD/BS*], or rank-2. In this scenario, the influence of the motor-induced interactions with the soft phantom may induce the agent to see some inclusion types as more similar to others, depending on which property is deemed more important.

To assess the performance of category formation in each experiment, we first need to match the clusters found by the KMC algorithm to any set of target classes for the phantom under analysis. We devise a cluster matching process based on maximal accuracy.

Given the previously computed guess vector $\mathbf{v}$ and classes $\mathbf{C}$, we first define a function Γ such that

$$\Gamma(\mathbf{v}, \mathbf{C}) = [x| \; x = \mathbf{C}_{\mathbf{v}_i} \text{ for } i \in [1, ..., N]] \tag{11}$$

where $\mathbf{v}_i$ is the i^{th} element in $\mathbf{v}$, $\mathbf{v}_i \in \mathbf{C}$, and $\mathbf{C}_{\mathbf{v}_i}$ is the $\mathbf{v}_i^{th}$ element in C. The function remaps the elements in $\mathbf{v}$ based on $\mathbf{C}$.

Given a target vector $\mathbf{t}$ we define a function Ψ to re-associate the classes in C such that the distance between the target and the guess vector is minimal, thus:

$$\Psi(\mathbf{v}, \mathbf{C}) = \underset{\mathbf{C}\,'}{\operatorname{argmin}} ||\Gamma(t, \mathbf{C}\,') - \mathbf{v}||$$

where $C\,' \in S(\mathbf{C})$, $S(C)$ is the set of all permutations of C, and $||\cdot||$ is the Euclidean norm of a vector. Finally we define the cluster-matching as:

$$\mathbf{CM}(\mathbf{v}, \mathbf{t}, \mathbf{C}) = \Gamma(\mathbf{v}, \; \Psi(\mathbf{v}, \mathbf{C})) \tag{12}$$

We use the cluster-matching process to re-associate the cluster memberships

$$\mathbf{v}\,' = \mathbf{CM}(\mathbf{v}, \mathbf{t}, \mathbf{C}). \tag{13}$$

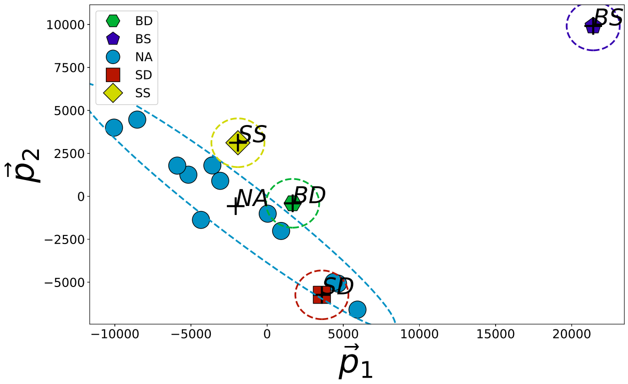

(a) $\Theta = \left\{ \begin{smallmatrix} 6.5 \\ 0 \end{smallmatrix} \right\}$

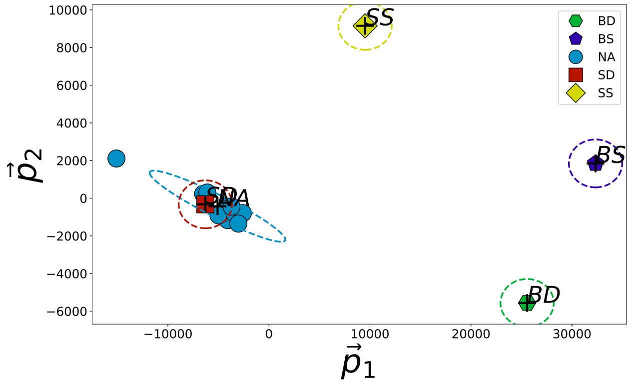

(b) $\Theta = \left\{ \begin{smallmatrix} 19.5 \\ 0 \end{smallmatrix} \right\}$

Fig. 14: The 2-dimensional projection of the tactile information generated from probing Ph-2 at varying depths. The ellipses correspond to the distributions of the clusters based on their true inclusion types, at a distance of 2 standard deviations from their respective cluster center.

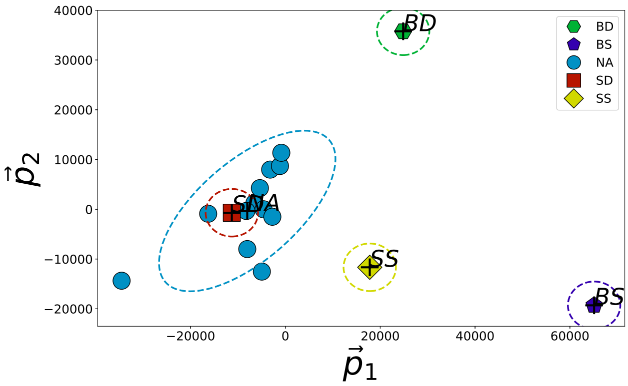

(a) $\Theta = \left\{ \begin{smallmatrix} 10 \\ 10 \end{smallmatrix} \right\}$

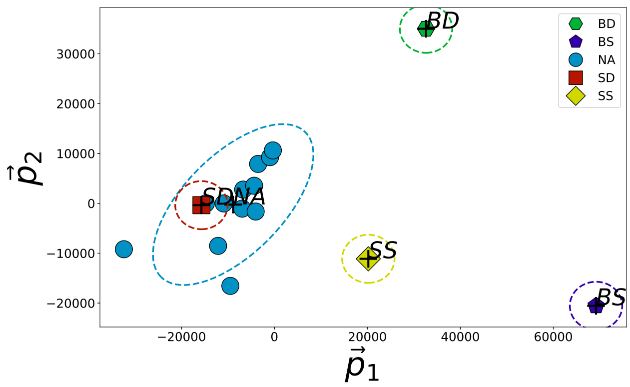

(b) $\Theta = \left\{ \begin{smallmatrix} 10 \\ 16 \end{smallmatrix} \right\}$

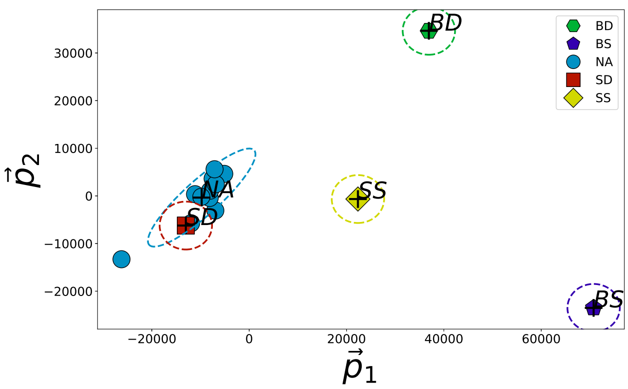

(c) $\Theta = \left\{ \begin{smallmatrix} 16 \\ 10 \end{smallmatrix} \right\}$

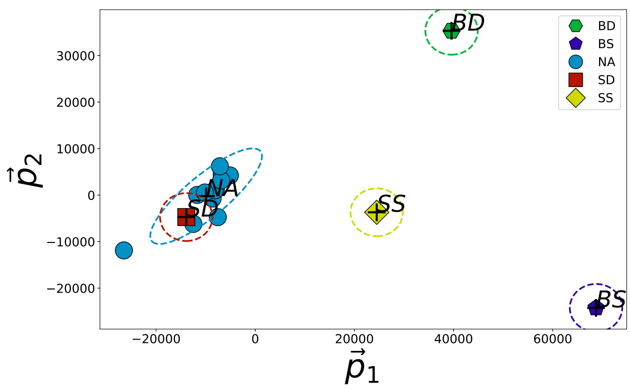

(d) $\Theta = \left\{ \begin{smallmatrix} 16 \\ 16 \end{smallmatrix} \right\}$

Fig. 15: The 2-dimensional projection of the tactile information generated from probing Ph-2 at varying depths and radii. The ellipses correspond to the distributions of the clusters based on their true inclusion types, at a distance of 2 standard deviations from their respective cluster center.

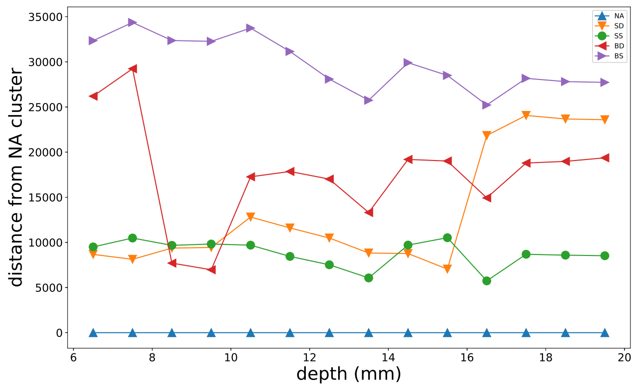

Fig. 16: The distance between the cluster-matched *NA* cluster and all matched clusters in the data. The data is captured when probing *Ph*-2 and , setting $r = 0$ and varying the d in Θ.

Here $\mathbf{v}'$ is a new vector maximizing accuracy for a particular task given (specified by the target vector $\mathbf{t}$). A vector $\mathbf{v} = [2\ 2\ 1\ 0\ 0]$ for a task $\mathbf{t} = [1\ 1\ 0\ 2\ 2]$, for example, would be re-associated as $\mathbf{v}' = [1\ 1\ 0\ 2\ 2]$. We utilize the cluster memberships in $\mathbf{v}'$ to compute each cluster center and retrieve the mutual distances between clusters.

In this analysis we consider two scenarios where we may want to associate the clusters by depth or size of inclusion, and use the *NA* type as ground zero, we thus consider the distance from the cluster-matched *NA* inclusion type and the remaining types (Fig. 16). As clear from Fig. 16, by duly interacting with the soft phantom, the distance between each cluster type and the *NA* cluster changes drastically. In this context, then, it is possible to induce a ranked understanding of robot's perceived similarities between different inclusion types by simply acting on the Θ parameters.

We demonstrate the ability to achieve similarity relationships of the kind previously described by finding the parameters for which the agent can rank the system based on rank-1 or rank-2. We perform the experiments in *Ph*-2, and we use the experimental data gathered through the probing of the soft phantom to find the parameters by which we can solve the ranking. We find the robot capable of abstracting similarities relationships according to rank-1 for $\Theta = \left\{ {9.5 \atop 0} \right\}$ (Fig. 17a), and according to rank-2 for $\Theta = \left\{ {15.5 \atop 0} \right\}$ (Fig. 17b).

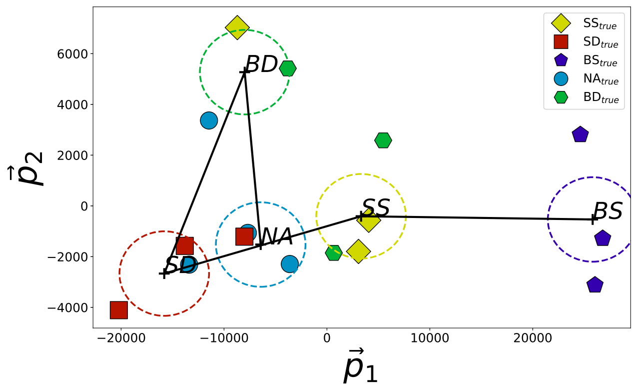

(a) *Ph*-2, $\Theta = \left\{ {9.5 \atop 0} \right\}$

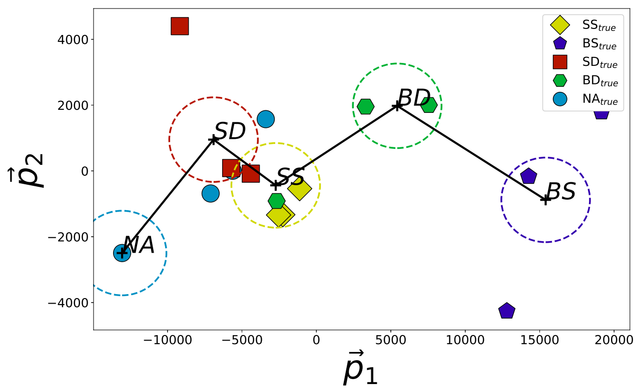

(b) *Ph*-2, $\Theta = \left\{ {9.5 \atop 0} \right\}$

Fig. 17: The emerging cluster similarities when changing the motion parameters and solving for either rank-1 i.e. [*NA*, *SD*/*BD*, *SS*/*BS*] (a) or rank-2 i.e. [*NA*, *SD*/*SS*, *BD*/*BS*] (b). Each dotted circle is placed on the cluster-matched, KMC found, cluster corresponding to the color coding in the legend.

5 Conclusion

In this paper we investigated the effects of various motion strategies to the response of a capacitive tactile sensor, for the task of detecting hard inclusions in a soft body. Actively choosing an interaction strategy, to optimize sensory reception for a specific task at hand, has the potential to be a powerful tool. Such tool could endow robots with the ability to dynamically filter properties of touched objects, actively helping in the completion of a task [2,15] even before the sensor information arrives to a central processing unit.

The experiments were performed by embedding a capacitive tactile sensor onto a 3D-printed end-effector, and probing two soft phantoms with various hard inclusions through different probing strategies. The sequential sensor data obtained through the probing of each area in the phantom was clustered, and the change in information due to each strategy observed and analyzed.

We found the amount of information retained after PCA projection to be highly dependent both on the probing strategy and the properties of the sample areas in interaction. More interestingly, we found that appropriate probing strategies can help retain information even when lacking a large quantity or good quality of it. Using the explained variance as a measure of information is useful in ensuring large amount of heterogeneity is kept in the data, but it is not capable of ensuring the quality of the information retained. In fact, it could be possible that the projection makes the information relative to highly distinct object, indistinguishable after projection. However, under the assumption of no prior knowledge of target labels, keeping variance in the data is usually a sensible choice.

Furthermore, we analyzed the impact due to motion on cognitive maps and extracted how the motion influenced the tactile information. Understanding the effects of motion to the perception of the probed areas is necessary to appropriately choose an interaction strategy that generates structure. To make full use of such effects, however, it would be ideal to instead be able to predict such change, before interaction takes place. Here, the change in position of each point within a cognitive map could be interpreted as a transformation in the same domain. The transformation function could be learned from initial interaction and used in future tasks to optimize the sensor response for a specific task. The transformation function, however, would not only be dependent on the motion parameters employed, but also on the properties of the sample objects in interaction, like demonstrated in the results.

Finally, it is possible to take categorization one step further and abstract similarities between object types from Cognitive Maps. Here we have shown that the physical interaction can drive the similarity relationship between objects. In an unsupervised scenario, the abstractions can be highly informative and can, for example, be useful to fix an ordering, via mutual distances, on the sensed object types. The object ordering can be purposefully fixed to the agent's advantage. In a real scenario a practitioner might diagnose the gravity of a detected inclusion based on various features. In our fictitious example we show how it is possible for an agent to prioritize over two features by simply changing the palpation strategy.

The findings shed some light in the motor-induced sensory reception of tactile information in the context of palpation diagnosis and we believe open new doors in the active use of motion-driven sensing for solving palpation tasks.

References

1. Bendtsen L, Jensen R, Jensen N, Olesen J (1995) Pressure-controlled palpation: a new technique which increases the reliability of manual palpation. Cephalalgia 15(3):205–210
2. Bohg J, Hausman K, Sankaran B, Brock O, Kragic D, Schaal S, Sukhatme GS (2017) Interactive perception: Leveraging action in perception and perception in action. IEEE Transactions on Robotics 33(6):1273–1291
3. Dahiya R, Metta G, Valle M, Sandini G (2010) Tactile sensing-from humans to humanoids. IEEE Trans on Robotics 26(1):1–20
4. Drimus A, Kootstra G, Bilberg A, Kragic D (2014) Design of a flexible tactile sensor for classification of rigid and deformable objects. Robotics and Autonomous Systems 62(1):3–15
5. Eberman LE, Finn ME (2010) Enhancing clinical evaluation skills: Palpation as the principal skill. Athletic Training Education Journal 5(4):170–175
6. Hoffmann M, Pfeifer R (2012) The implications of embodiment for behavior and cognition: animal and robotic case studies. arXiv preprint arXiv:12020440
7. Iida F, Nurzaman S (2016) Adaptation of sensor morphology: An integrative view of perception from biologically inspired robotics perspective 6:20160016
8. Konstantinova J, Jiang A, Althoefer K, Dasgupta P, Nanayakkara T (2014) Implementation of tactile sensing for palpation in robot-assisted minimally invasive surgery: A review. IEEE Sensors Journal 14(8):2490–2501
9. Konstantinova J, Li M, Mehra G, Dasgupta P, Althoefer K, Nanayakkara T (2014) Behavioral characteristics of manual palpation to localize hard nodules in soft tissues. IEEE Transactions on Biomedical Engineering 61(6):1651–1659
10. Konstantinova J, Cotugno G, Dasgupta P, Althoefer K, Nanayakkara T (2017) Palpation force modulation strategies to identify hard regions in soft tissue organs. PloS one 12(2):e0171706
11. Lloyd S (1982) Least squares quantization in pcm. IEEE Trans Inform Theory 28(2):129–137, DOI 10.1109/TIT.1982.1056489
12. Lungarella M, Pegors T, Bulwinkle D, Sporns O (2005) Methods for quantifying the informational structure of sensory and motor data. Neuroinformatics 3(3):243–262
13. McLaughlin ML, Hespanha JP, Sukhatme GS (2002) Introduction to haptics
14. Nolfi S, Marocco D (2002) Active perception: A sensorimotor account of object categorization. In: From animals to animats 7: Proceedings of the VII international conference on simulation of adaptive behavior, et al., Cambridge, MA, pp 266–271
15. Olsson L, Nehaniv CL, Polani D (2004) Sensory channel grouping and structure from uninterpreted sensor data. In: Evolvable Hardware, 2004. Pro-

ceedings. 2004 NASA/DoD Conference on, IEEE, pp 153–160
16. Pfeifer R, Scheier C (1997) Sensorymotor coordination: The metaphor and beyond. Robotics and autonomous systems 20(2-4):157–178
17. Pfeifer R, Lungarella M, Sporns O, Kuniyoshi Y (2007) On the information theoretic implications of embodiment–principles and methods. In: 50 years of artificial intelligence, Springer, pp 76–86
18. Puangmali P, Althoefer K, Seneviratne L, Murphy D, Dasgupta P (2008) State-of-the-art in force and tactile sensing for minimally invasive surgery. IEEE Sensors Journal 4(8):371–381
19. Rousseeuw PJ (1987) Silhouettes: a graphical aid to the interpretation and validation of cluster analysis. Journal of computational and applied mathematics 20:53–65
20. Schmitz A, Maiolino P, Maggiali M, Natale L, Cannata G, Metta G (2011) Methods and Technologies for the Implementation of Large-Scale Robot Tactile Sensors. IEEE Trans on Robotics 27(3):389–400, DOI 10.1109/TRO.2011.2132930
21. Scimeca L, Maiolino P, Iida F (2018) Soft morphological processing of tactile stimuli for autonomous category formation. IEEE International Conference on Soft Robotics, Robosoft
22. Sornkarn N, Nanayakkara T (2016) The efficacy of interaction behavior and internal stiffness control for embodied information gain in haptic perception. In: Robotics and Automation (ICRA), 2016 IEEE International Conference on, IEEE, pp 2657–2662
23. Sporns O, Lungarella M (2006) Evolving coordinated behavior by maximizing information structure. In: Artificial life X: proceedings of the tenth international conference on the simulation and synthesis of living systems, Citeseer, vol 10, p 323
24. Tipping ME, Bishop CM (1999) Probabilistic principal component analysis. Journal of the Royal Statistical Society: Series B (Statistical Methodology) 61(3):611–622, DOI 10.1111/1467-9868.00196
25. Tuci E, Massera G, Nolfi S (2009) On the dynamics of active categorisation of different objects shape through tactile sensors. In: European Conference on Artificial Life, Springer, pp 124–131
26. Wang N, Gerling GJ, Childress RM, Martin ML (2010) Quantifying palpation techniques in relation to performance in a clinical prostate exam. IEEE Transactions on Information Technology in Biomedicine 14(4):1088–1097
27. Yen PL (2003) Palpation sensitivity analysis of exploring hard objects under soft tissue. In: Advanced Intelligent Mechatronics, 2003. AIM 2003. Proceedings. 2003 IEEE/ASME International Conference on, IEEE, vol 2, pp 1102–1106